An investigation of the inter-molecular interaction, solid-state properties and dissolution properties of mixed copovidone hot-melt extruded solid dispersions

Dean Hurley[1, 2], David Carter[1], Ng Lawrence[1], Mark Davis[2], Gavin M. Walker[2], John G. Lyons[1], Clement L. Higginbotham[1, 2*]

[1]Materials Research Institute, Athlone Institute of Technology, Athlone, Ireland

[2]Synthesis and Solid State Pharmaceutical Centre (SSPC), Bernal Institute, University of Limerick, Limerick, Ireland.

Correspondence to: Clement L. Higginbotham

Tel: +353-(0)-90-6468050

Email: chigginbotham@ait.ie

Abstract

Previous research has focused on spray dried quaternary mixtures which due to the addition of a surfactant affected the physical stability and amorphous stability of selected model drugs. Very little research has focused on how inter-molecular interactions play a role in the successful formulation of hot-melt extruded quaternary amorphous blends and how they affect physical stability and solubility of amorphous solid dispersions (ASDs). Therefore the aim of this study was to investigate the role of inter-molecular interactions and their effect on the solid-state and dissolution properties of mixed copovidone amorphous solid dispersions (ASDs). The polymeric copovidone carriers used in this study was Poly (vinylpyrrolidone-vinyl acetate copolymer) and Plasdone S-630 (PL-S630) which in terms of monographs are the same, however they have different solid-state and dissolution properties. The ASDs showed a significantly higher dissolution rate compared to amorphous and pure INM in pH buffer 1.2 with a kinetic solubility of 24 µg/ml. The stability data showed that INM remained amorphous in solid solutions with PVP VA64 and Plasdone S-630, except for the higher drug loads. It was concluded that % drug loading did have a significant effect on the solubility of INM due to recrystallization at higher drug loads.

Keywords

Solid dispersion, crystallization, glass transition, extrusion, solubility, amorphous

1.1. Introduction

The vast majority of new chemical API's are poorly water soluble and as a result pose many challenges for formulation scientists in pharmaceutical industries [1]. Various methods such as the formulation of pro-drugs, micronization and the formulation of amorphous solid dispersions (ASDs) have been developed to overcome the solubility barrier associated with poorly water soluble drugs [2–5]. The formulation of thermodynamic high energy amorphous form of crystalline APIs is a promising method to improve the solubility of BCS class II drugs [6]. As amorphous APIs have a higher free energy, they can exhibit a dissolution rate and extent many times greater than the crystalline equivalent. However, the thermodynamic high energy amorphous form is prone to recrystallization and physically unstable [7]. Recrystallization of the API has two stages, the first step is nucleation and the second step is crystal growth [8]. Nucleation occurs at a lower temperature, while crystal growth requires significantly higher temperatures. Nucleation is the formation of small aggregates of a critical size. This is the rate-limiting step and the rate of nucleation depends on the activation energy or crystallization activation energy [9,10]. Crystal growth is the diffusion of solute molecules to the surface of the nuclei or crystal lattice. Therefore preventing nucleation and crystal growth is necessary in order to prevent recrystallization and physical instability [7,8].

To date predicting inter-molecular interactions is of great interest not just in the pharmaceutical industry but also in solid dispersion formulation. The process involves the interaction between a polymeric matrix and a small molecule drug. The thermodynamics of mixing states that for an interaction to exist between a polymer and API, there must be a negative change in the free energy of mixing [11].

This change in the free energy of mixing is related to the entropic and enthalpy contributions according to the following equation (Eq. 1).

$$\Delta G_{mix} = \Delta H_{mix} - T \times \Delta S_{mix}$$

ΔG_{mix} is the Gibbs free energy, ΔH_{mix} is enthalpy of mixing, ΔS_{mix} is the entropy of mixing and T is the absolute temperature. This negative change in free energy is spontaneous due to the increase in the entropy of mixing. However the presence of repulsive and cohesive inter- and intramolecular forces (e.g. dipole-dipole interaction, dispersion force and hydrogen bond interaction) which are present within the solid dispersion system make the interaction between polymer and drug more complicated [12].

Hydrogen bond formation between the polymeric carrier and the API is thought to play a significant role in preventing recrystallization in amorphous drugs [13,14]. The most common technique used to identify

hydrogen bonds between the polymer and API has been FT-IR spectroscopy [14]. Taylor and Zografi. (1997) detected the inter-molecular interaction between the carboxylic acid moiety of PVP and indomethacin using this conventional technique [13]. Many other researchers also detected the presence of hydrogen bonds between the APIs felodipine and nifedipine using PVP as a polymeric carrier in ASDs [15].

High resolution ^{13}C solid-state NMR spectroscopy has often been used to examine hydrogen bonding inter-molecular interactions in solid dispersions [16]. Miyoshi and many other researchers found three types of carboxylic acid groups in amorphous solid dispersions of various polymeric carriers such as poly (ethylene oxide) (PEO) and poly (acrylic acid) (PAA). These carboxylic acid groups were assigned as follows 1) interpolymer hydrogen bonding between PEO and PAA, 2) hydrogen bonded dimers associated with PAA and 3) non-hydrogen bonding interactions [16]. However Yuan et al. (2015) reported that they could not distinguish between the amide C=O carbonyl of INM and PVP VA64/PVP using labelled compounds via solid state NMR spectroscopy [17]. Therefore Raman spectroscopy will be used in this study as an alternative technique to understand the nature of interaction between PVP VA64 and INM in this study in conjunction with ATR-FTIR spectroscopy.

Successful formulation of these systems requires therefore the formation of a homogenous system and physical stability must be considered [18]. It has been reported that multi-component solid dispersions such as quaternary and ternary ASDs can result in phase separation as a result of incorporating surfactants within binary and ternary ASDs [19]. Also recrystallization of an amorphized additive has been reported to retard drug release within ASDs [20]. Previous research has focused on spray dried quaternary mixtures which, due to the addition of a surfactant, affected the physical stability, amorphous stability and dissolution of selected model drugs[18]. Very little research has focused on how inter-molecular interactions play a role in the successful formulation of hot-melt extruded quaternary amorphous blends and how they affect physical stability and solubility of amorphous solid dispersions (ASDs). Therefore this study will focus on the role of inter-molecular interactions and their effect on the solid-state and dissolution properties of mixed copovidone hot-melt extruded quaternary solid dispersions. Poloxamer 407 (P407) will be used as a surfactant to improve solubility of a selected model drug and prevent recrystallization. Also, ternary (drug-polymer-surfactant) and binary (INM-P407) ASDs will be prepared for comparison purposes.

In terms of monographs, PL-S630 and PVP VA64 are the same product. However these co-polymers are manufactured from two different manufacturers, and therefore have different solid-state and dissolution properties as a result of their manufacturing process. Differences in the manufacturing process from different suppliers of copovidone can influence the properties of the copovidone produced. Some of these properties may be critical material attributes for the manufacturing process or performance of a drug

product. For example different supplier's products may have different glass transition temperatures. Therefore this is why PL-S630 and PVP VA64 was chosen for this study, and very little has been reported in literature on the comparison of PL-S630 and PVP VA64 regarding their solid-state and dissolution properties.

Indomethacin (INM) was selected as a model drug due it to poorly-water soluble properties. The role of drug-polymer interaction and anti-plasticization in enhancing supersaturation of INM was investigated. This is a continuation of previous work carried out to understand the interaction between INM and P407 in preventing recrystallization of INM and the type of interaction between INM-PVP VA64 ASDs. The ASDs were characterized by ATR-FTIR Spectroscopy, Raman spectroscopy, X-ray powder diffraction (XRPD), phase solubility studies and *in-vitro* dissolution studies. This study will aid the understanding of the use of surfactants in ASDs to aid formulation scientists in the design of multi-component amorphous drug/solid dispersion systems.

2.1 Materials and Methods

2.1.1 Materials

Crystalline γ-indomethacin (1-(4-Chlorobenzoyl)-5-methoxy-2-methyl-3-indoleacetic acid) (INM), purchased from Tokyo Chemical Industry (TCI) (Oxford Science Park, UK) (N.V.) (T_m 160 °C T_g 42 °C), was used as a model drug [21]. INM has a kinetic solubility of 1.5 µg/ml at pH 1.2[21]. P407 (T_m 55 °C, T_g -67 °C), a hydrophilic non-ionic surfactant and PVP VA64 (T_m 86.16 °C, T_g 106 °C), were purchased from BASF Europe GmbH (Burgbernheim, Germany). PL-S630 (T_m 140 °C, T_g 107 °C), was received as a gift from Ashland Specialties Ltd, (UK). All other reagents and chemicals were purchased from Sigma Aldrich (Wicklow, Ireland) and were of analytical reagent grade.

2.1.2 Preparation of physical mixtures

8 different combinations of all four components were studied and 40 g total powder was used for each sample. Powders were weighed and mixed thoroughly in a mortar and pestle for five minutes according to the compositions detailed in Table 2 and compared against various ternary mixtures (Table 3). Also binary ASDs were using INM and P407 as a control. The % drug-polymer composition used for binary ASDs are as follows 10/90, 30/70, 50/50 and 70/30% INM-P407. Amorphous INM (aINM) was prepared by heating to 160 °C in a stainless steel beaker using a hotplate and quench cooling using liquid nitrogen.

2.1.3 Hot melt extrusion

Hot melt extrusion was performed using a co-rotating Prism 16mm Twin-screw extruder (Thermo Fisher Scientific, USA) with a 2mm diameter die and a length to diameter (L/D) ratio of 15/1. Screws contained all-conveying elements and a screw speed of 100 RPM was used. The extruder was split into three heating zones which, from feeding zone to the die, had set points of 140 and 160 °C. On exiting the die the extrudates were allowed to cool to 25 °C then ground under liquid nitrogen in a mortar and pestle and passed through a 200 µm sieve to obtain an appropriately sized fraction for further studies. All samples were pre-dried using phosphorus pentoxide prior to analysis to remove any significant moisture.

Calculation of Hansen solubility parameters (δ) and drug-polymer interaction factor (χ)

Hansen solubility parameters (δ) of both the drug and polymers were calculated by considering their chemical structure orientations and their molecular weights. In order to determine drug-polymer miscibility,

the solubility parameters were calculated using the combined group contribution methods of Van Krevelen-Hoftyzer and Fedors [7]. These are expressed by the following equation (Eq) 2:

$$\delta^2 = \delta^2_d + \delta^2_p + \delta^2_h \qquad \text{Eq. (2).}$$

Where,

$$\delta_d = \frac{\Sigma F_{di}}{V},\ \delta_p = \frac{(\Sigma F_{pi}{}^2)}{V}^{1/2},\ \delta_h = \left(\frac{\Sigma F_{hi}}{V}\right)^{1/2}$$

where *i* is the functional group within the molecule, δ is the total solubility parameter, δ_d is the contribution from dispersion forces, δ_p is the contribution of polar interactions, δ_h is the contribution of hydrogen bonding, F_di is the molar attraction constant due to molar dispersion forces, F_pi is the molar attraction constant due to molar polarization forces, E_hi is the hydrogen bonding energy and *V* is the molar volume [22].

The drug-polymer interaction parameter, χ, using the solubility parameter difference between the drug and polymer, can be estimated by a method developed by Hildebrand and Scott [23].

This is expressed as follows;

$$\chi = \frac{Vo}{RT}(\delta_{drug} - \delta_{polymer})^2 \qquad \text{Eq. (3).}$$

where *V*o is the volume of the lattice site, *R* is the gas constant and *T* is the absolute temperature.

2.1.4 ATR-FTIR Spectroscopy

ATR-FTIR spectra were collected using a Perkin Elmer, Spectrum One apparatus fitted with a universal ATR sampling accessory. Data was collected in the spectral range of 4000-420cm^{-1}, utilizing a 16 scan per sample cycle and a fixed universal compression force of 80N. Subsequent analysis was carried out using Spectrum software.

2.1.5 Raman Spectroscopy

Raman spectra were obtained using a Reninshaw invia Raman confocal microscope (Renishaw Instruments, Gloucestershire**,** UK) coupled to a motorised stage. Raman scattered light from a 785 nm laser, operating at 300 Mw using 100% laser power. Spectra were collected between 100 and 3200 cm^{-1}, and with a total collection (acquisition) time of 10 seconds. The lens used was a x20 lens, with a laser spot size of 50 µm. The beam path grating used was 1200 l/mm (633/780).

2.1.6 X-ray powder diffraction (XRPD)

X-ray diffraction spectra were collected using a Philips PANalytical X'Pert MPD Pro with PW3064 sample spinner. The dried granules were gently ground using a pestle and mortar and placed on zero-background silica disks. The diffraction pattern was collected between 5 and 40° (2θ) with a step size of 0.0167°, a counting time of 29.845 s, and a sample rotation of 15 rpm using PANalytical Data Collector, version 2.0. The source was Cu Kα (λ = 1.5418 Å), the accelerating voltage was 40 kV, and the anode current was 35 mA. A fixed divergence slit of ¼" and a 0.020 mm nickel filter were used

2.1.7 Phase solubility Studies

Solubility studies of pure drug and polymers were performed in triplicate using the method reported by Higuchi and Connors (Higuchi *et al*. 1965) in pH buffer 1.2 [24]. An excess amount of INM was added to aqueous solutions of each carrier to increasing concentrations of both polymeric carriers in 10 ml volumetric flasks. The suspensions were maintained at 37 °C for 24 h. This duration was previously tested to be sufficient to reach equilibrium.

2ml aliquots were withdrawn and were filtered through 25mm Millex - LCR PTFE hydrophilic syringe filters (0.45 µm, Merck Millipore LTD, Ireland). The filtrates were suitably diluted if required and analyzed, spectrophotometrically for the dissolved drug at 320 nm. Shaking was continued until three consecutive readings were performed. The apparent 1:1 stability constant Ka was calculated from the phase solubility graph using the following equation:

$$K_a = \frac{\text{Slope}}{\text{So (1-slope)}} \qquad \text{Eq. (4).}$$

Where So is the intrinsic aqueous solubility of INM. The Gibbs free energy of transfer (ΔG^0_{tr}) of INM from pure water to the aqueous solution of carrier was calculated by the equation below.

$$\Delta G^0_{tr} = -2.303\ RT \log S_o/S_s \qquad \text{Eq. (5).}$$

where S_O/S_S is the ratio of molar solubility of INM in aqueous solutions of carrier to that of the same medium without carrier.

Also the solubility of the various ASD formulations and physical mixtures were performed in pH buffer 1.2. An excess amount of ASD formulation was mixed with 10ml of pH buffer 1.2 and was shaken at 37 °C in a mechanical shaker for 24 hours. 2ml aliquots were withdrawn and were filtered through 25mm Millex - LCR PTFE hydrophilic syringe filters (0.45 µm, Merck Millipore LTD, Ireland). The filtrates were suitably diluted if required and analyzed, spectrophotometrically for the dissolved drug at 320 nm as previously mentioned.

2.1.8 In-Vitro Dissolution Studies

The release rate of INM from ASDs was determined under non-sink conditions using United States Pharmacopeia (USP) dissolution testing apparatus 1 (basket method) (Distek 50947, USA) with a paddle speed of 50 rpm. The dissolution test was performed using 900 ml of pH buffer 1.2 at a temperature of 37 ± 0.5 °C. A formulation equivalent to 100 mg of INM in ASDs was placed in dissolution medium, with 5 ml aliquots withdrawn at predetermined time intervals (0, 10, 17, 24, 45 minutes and 1, 2 and 3 hours), and filtered through a 25mm Millex - LCR PTFE hydrophilic syringe filter (0.45 µm, Merck Millipore LTD, Ireland). At each time point, the same volume of fresh medium was replaced as withdrawn.

The concentration of INM in each sample was determined using a UV-1280 UV-Vis spectrophotometer (Shimadzu, Japan) and a standard calibration curve. Fresh dissolution medium was used as a blank. Pure INM and amorphous INM were used as controls. The concentration of INM dissolved for each formulation (n =3) was plotted as a function of dissolution time with data being expressed as the average ± standard deviation of replicate absorbance measurements.

2.1.9 Statistical Analysis

The drug dissolution profiles of all ASD formulations were compared using an analysis of variance (ANOVA) statistical test. The impact of the amorphous form on the area under the curve (AUC) was statistically examined using (ANOVA) (GraphPad Prism version 5.03 for Windows, GraphPad Software, San Diego, CA). Post-hoc comparisons of the means were performed using Tukey's Multiple Comparison test. A significance level of * $p < 0.05$ was accepted to denote significance in all cases.

2.1.10 Accelerated amorphous stability studies

Stability studies were conducted under accelerated conditions (40 °C, 75% relative humidity) for 5 months by placing ASDs in open glass vials which were stored in a desiccator which contained a saturated solution of sodium chloride to generate a relative humidity of 75% RH. The relative humidity inside the desiccator was checked regularly using a thermohygrometer. The stored ASDs were dried over phosphorus pentoxide for at least 24 hours prior to hyper analysis to remove the significant moisture endotherm exhibited in non-dried samples.

Hyper DSC studies were conducted on a PerkinElmer DSC 8500 equipped with a refrigerated cooling accessory (PerkinElmer, UK). Helium, 30 mL/min, was used as purge gas. The instrument was calibrated using a heating rate of 100 °C/min using high purity indium to standardize the temperature and heat flow signal. Then 1.0−2.5 mg samples were weighed and placed in crimped DSC pans. Samples were ramped

from -10 to 180 °C at 100 °C/min. The analysis was carried out using PerkinElmer Pyris Thermal Analysis software, version 10.1 and any numerical values reported are the average ± SD of three independently prepared samples.

3.1 Results and Discussion

3.1.1 Hansen solubility parameters (δ) and drug-polymer interaction factor (χ)

The calculation of the drug-polymer interaction factor and Hansen solubility parameters heavily depend on the various types of intermolecular interactions and the various cohesive and repulsive intra- and intermolecular forces and molecular volumes of each of the components. The examination of both polymers and drug used in this study in Figure 1, indicate that they are all polar and thus are able to be involved in hydrogen bonding. All data in this study for the calculations of the interaction factor and solubility parameters was further examined using ATR-FTIR spectroscopy, Raman spectroscopy, XRPD, phase solubility studies, *in-vitro* dissolution studies and accelerated stability studies in conjunction with hyper DSC. Maniruzzaman *et al*. (2015) reported that using the lattice-based Flory-Huggins (F-H) theory to describe interactions between drug and polymer is limited as it doesn't take into account the multiple interactions in drug-polymer systems [12]. So the Hansen solubility parameters developed by Van Krevelen and Hoftyzer group contribution were used as an alternative to understand the nature of interactions that occur within these systems.

In this study the Hildebrand-Scott method was used and is the theoretical method applied to determine F-H interaction parameters and is based on the Hansen solubility parameters developed by Van Krevelen and Hoftyzer group contribution. The value of χ, refers to the square of the difference in solubility parameters calculated by Van Krevelen and Hoftyzer group contribution method at 25 °C (Table 3). A numerical value close to zero of χ shows favourable intermolecular interactions within drug-polymer ASD systems [23]. This was the case as all values were close to zero. However, the calculated results from this method does not show the type of interactions that takes place within the drug-polymer system [12].

Based upon their chemical structures, the Hansen solubility parameters (δ) for INM, PVP VA64, PL- S630 and P407 were calculated to be 23.00 $MPa^{1/2}$, 26.40 $MPa^{1/2}$, 26.40 $MPa^{1/2}$ and 25.50 $MPa^{1/2}$ respectively **as shown in Table 3**. Recent literature has reported that favourable intermolecular interactions and a uniform

phase will result if the difference in the δ values between each of the components (Δδ) is less than 7 $MPa^{1/2}$ as shown in Table 3. This is because the energy of mixing from intermolecular interactions is balanced with the energy of mixing from intramolecular interactions [25]. Unfavourable intermolecular interactions and phase separation and/or recrystallization will result if $\Delta\delta > 7$ $MPa^{1/2}$ [26]. In this study, Δδ between all polymers and INM was less than 7 $MPa^{1/2}$ and in theory are likely to be miscible and more likely to achieve the amorphous state.

It is important to note that the calculated molar attraction constant as a result of hydrogen bonding for INM was relatively high (10.37 $MPa^{1/2}$) and quite close to the values calculated for the polymeric carriers (PVP VA64: 11.86 $MPa^{1/2}$ and PL-S630: 11.86 $MPa^{1/2}$). These high values as a result of hydrogen bonding may play a significant role for the possible drug-polymer intermolecular interactions that occurs during the conversion from the crystalline to amorphous state. Maniruzzaman *et al*. 2015 prepared hot-melt extruded solid dispersions using the BCS class II drug Verapamil HCL and BCS class I drug Cetirizine HCL and had molar attraction constants of 6.95 $MPa^{1/2}$ and 9.60 $MPa^{1/2}$ reported that due to their high molar attraction constants were able to participate in hydrogen bonding [12]. These values were similar to the molar attraction constant for INM. However, Hansen solubility parameters and F-H interaction parameters are only theoretical and drug-polymer miscibility between INM and polymers was further examined using ATR-FTIR spectroscopy, Raman spectroscopy, XRPD, phase solubility studies, *in-vitro* dissolution studies and accelerated stability studies in conjunction with **hyper** DSC.

3.1.2 XRPD Studies

The physical state of pure and amorphous INM, pure P407, pure PVP VA64/PL-S630 and ASD formulations were further examined by XRPD analysis. The XRPD patterns of pure drug, polymers and ASD formulations are shown in Figures 2(a) and 2(b). XRPD pattern for pure INM had several diffraction peaks due to the crystalline nature of the drug. The main principal crystalline peaks occurred at diffraction angles (2θ) at 11.72°, 17.11°, 19.67°, 20.93°, 21.90°, 24.03°, 26.64° and 29.43° as shown in Figure 2(a). These values were similar to the values reported in literature for this drug [27]. The XRPD pattern of PVP VA64 and PL-S630 were amorphous in nature.

This can be a seen by a slight amorphous halo raised above the baseline. P407 which is semi-crystalline in nature contained two strong principal diffraction peaks at 19.26° and 23.51° respectively due to its semi-crystalline structure. XRPD analysis of the ASD formulations confirmed the amorphous nature of INM within all ASD formulations due to the slight halo raised above the baseline, due to the lack of any sharp, well-defined peaks in the diffractograms as shown in Figure 2 (b). However, the 50% and 70% INM SD formulations were not completely amorphous due to the high INM loading as expected.

For all other SD formulations both ternary and quaternary ASDs, the semi-crystalline peaks associated with P407 was present, compared to the SD formulations reported by Gumaste *et al*.(2016)[28] in which poloxamer was converted to its amorphous form. However in the XRPD diffractograms of the 5% P407 loading ASD formulations, the semi-crystalline peaks of P407 appear at much weaker intensity compared to the 15% P407 loading samples.

This may be due to the fact that the physical interaction from P407 is much greater at high poloxamer loadings. The conversion from the crystalline to the amorphous form was a result of the possible intermolecular interactions mainly hydrogen bonding and thus formation of molecular solid dispersions. ATR-FTIR and Raman spectroscopy was used to elucidate the type and mechanism of interaction.

3.1.3 ATR-FTIR Spectroscopic Studies

ATR-FTIR spectroscopy was used to examine the intermolecular interactions for the all ASD formulations and to confirm the amorphous or crystalline nature of the API within the ASD formulations. The wavenumbers identified in this study for ATR-FTIR spectroscopy are similar to the values reported in literature. Crystalline INM was characterized by principal absorption peaks and showed two strong C=O bands at 1714.00 cm^{-1} (free C=O of carboxylic acid) and 1690.00 cm^{-1} (acid-acid dimer C=O stretch) respectively which are non-hydrogen bonding (Figure 3 (a)) [13]. The hydrogen-bonded O-H stretch of the acid is shown in Figure 3 is superimposed on the sharp C-H stretches, as recent literature has shown that the free carboxylic acid O-H stretch can exist as dimers due to hydrogen bonding [21]. PVP VA64 and PL-S630 had two strong principal peaks at 1731.00 cm^{-1} (C=O stretch of the vinyl acetate) and 1672.00 cm^{-1} (amide carbonyl C=O stretch) as shown in Figure 3 (b) [29]. In the ATR-FTIR reference spectrum of amorphous INM, the above named peaks shifted to 1707.00 cm^{-1} and 1679.00 cm^{-1} respectively due to conversion to its amorphous form [30] as shown in Figure 5, as a result do not align with the polymer peaks. See Tables 6-9 in supporting information for ATR-FTIR spectra interpretation.

The ATR-FTIR of all the ASD formulations with PL-S630, PVP VA64 and P407, amorphous INM was present and there was evidence of intermolecular interaction i.e. hydrogen bonding due to the shift of the amide carbonyl of PVP VA64/PL-S630 from 1672.00 cm^{-1} to 1680 cm^{-1} (Figure 4) and (Figure 3 (b)) **[29]**. There was no shift observed in the C=O of the vinyl acetate carbonyl of PVP VA64/PL-S630 in the ATR-FTIR spectra, however in the Raman spectra it must be noted that there was a shift in the vinyl acetate C=O carbonyl in all ASD formulations, however the quaternary ASD formulations had the greatest shift as shown in Figure 7. This is very significant as most literature states that the vinyl acetate C=O carbonyl is a weak hydrogen bond acceptor which was reported by Yuan *et al*. (2015) [17]. Any poloxamer peaks present in

the pure P407 sample were not present in the ATR-FTIR spectra of the SD formulations as shown in Figure 3 (c). This may indicate that P407 possibly has no molecular interaction with INM [31].

3.1.4 Raman Spectroscopic Analysis

Raman analyses was carried out **to further explore the hydrogen bonding interaction** between INM, PVP VA64, P407 and PL-S630 in the multi-component solid dispersions prepared by the HME process. Raman spectroscopy is complimentary to ATR-FTIR spectroscopy, and it is quite useful for the analysis of ASDs. Hydrogen bonding was the predicted mechanism of interaction due to high molar attraction constant of INM calculated using the Hansen solubility parameters and polarity of the drug-polymer mixtures. APIs normally tend to be conjugated or aromatic compounds which have strong Raman signals, while excipients have much weaker Raman signals and/or spectra. Similar to the ATR-FTIR studies, Raman spectroscopy showed potential intermolecular interaction between INM and polymeric carriers due to a shift in the amide carbonyl of PVP VA64 and PL-S630. The PVP VA64 amide carbonyl (νC=O) peak at 1673.00 cm^{-1} shifted to 1680.00 cm^{-1} in ASD samples due to hydrogen bonding interaction with the –OH group of INM as a result of hot melt extrusion as shown in Figure 6.

The acid νC=O present at 1702.00 cm^{-1} (free C=O of carboxylic acid) of INM completely disappears in the Raman spectra of the ternary and quaternary ASD formulations as a result of low intensity of INM. Based on the Raman spectra in Figure 6, none of peaks identified in the Raman spectra of amorphous INM were present in the Raman spectra of the ASD formulations. It must be noted even though a hydrogen bond shift was observed in all ASD formulations, the quaternary ASD formulations had a much greater shift as a result of the mixed copovidone present in the quaternary mixtures as shown in Figure 7. However small differences in the intensity and shifts in the peak positions were observed as a result of the HME process in the region of carbonyl group peaks (1660–1670 cm^{-1}). In summary, the ATR-FTIR and Raman analyses suggest that similar hydrogen bonding interactions were achieved in solid dispersions prepared by the HME process (Figure 3). The Raman analysis confirmed the ATR-FTIR results indicating hydrogen bonding interaction occurred between INM and PVP VA64/Plasdone S-630 as expected and confirmed that the drug and polymer were indeed miscible as predicted by the Hansen solubility parameters. See Tables 10-13 in supporting information for Raman spectra interpretation.

3.1.5 Phase Solubility Studies

INM shows a pH dependent solubility and is a weak acid with a pKa of 4.5. As the pH increases the kinetic solubility of INM increases. Pure INM shows a solubility of 1.5 µg/ml in pH 1.2 [21]. PVP VA64 and PL-S630 are non-ionic polymers and possess a pH independent solubility. In this study, solubility studies were performed in pH buffer 1.2. The kinetic solubility of INM from the various quaternary ASD formulations

are shown in Table 4. Also, a phase solubility plot of solubility of INM (µg/ml) against polymer concentration (% w/v) was drawn and exhibited a linear relationship in the chosen polymer concentration range that was examined. With regards to Figure 8, the Gibbs free energy values decreased as the % polymeric carrier loading decreased as shown in Table 4, which indicates that the drug solubilization process was indeed spontaneous [32]. The process is spontaneous due to the increase of ΔS_{mix} in mixing (due to increase in randomness) [12]. According to the first condition of the thermodynamics of mixing, for a drug and polymer to interact there must a negative change in the free energy of mixing.

The entropy of mixing is always favoured for drug-polymer ASD mixtures. The phase solubility plot shown in Figure 8 was an A-type phase solubility profile which shows that the kinetic solubility of INM increases with increasing polymer concentration. When a complex is first-order in nature with respect to ligand (polymeric carrier) and linear with respect to the substrate (API), hence the AL-type phase solubility curve is obtained [33]. For the ASD formulations, after 24 hours the quaternary ASD formulations had the highest kinetic solubility with a value of 76.30 µg/ml (Quart SD1) with 10% INM loading as shown in Table 4. The physical mixtures with the exception of PVP VA64 SD1, PL-S630 SD1 and Quart SD1 had a greater solubility for INM compared to the ASD formulations. This may have been due to recrystallization of INM due to high loading of P407 in the ASD formulations.

This is a significant improvement in the solubility of INM compared to the solubility reported by Chokshi *et al*. (2008) who reported that the maximum solubility of INM achieved after 24 and 72 hours was 10µg/ml and 30 µg/ml respectively, using 30, 50 and 70% INM loading. It also has been reported in literature that high poloxamer loading at high drug loads can retard drug release as a result of the gelling properties of poloxamer at high drug concentrations.

Physical mixtures tend to have a higher solubility because when the drug-polymer mixtures in the dry state are dispersed in aqueous solutions of polymer, polymeric particles hydrate rapidly due hydrophilic nature of P407 within polymer solutions resulting in the increased wettability of the drug particles [31]. This is related to surface activity and wetting effect which results in reduced agglomeration and solubilizing effect of P407. The kinetic solubility of the mixed PVP VA64 and PL-S630 systems was significantly higher than the ternary systems (Table 5). This may be due to greater vinyl acetate hydrogen bonding interaction as shown in Figure 7 in quaternary ASD formulations.

3.1.6 *In-vitro* dissolution studies

To further understand how the intermolecular interactions within multi-component i.e. quaternary and ternary ASDs affect the INM dissolution profile in pH buffer 1.2, *in-vitro* dissolution experiments were performed under non-sink conditions. The aim of this study was to examine the synergistic effect of the

various polymer combinations within ASDs and how it affected the maintenance of INM supersaturation. Pure INM and amorphous INM were also used as a control. The area under the curve (AUC) was calculated as a measure of the length of time that the supersaturated concentration could be maintained or achieved i.e. a measure of the supersaturated concentration [34]. The AUC was used to compare the solubility of INM between selected ASD formulations and pure/amorphous INM. Particle size was controlled in this study, the initial drug dosage within the dissolution vessels was 100mg as the particle size of each formulation was 200 microns as they were sieved prior to analysis.

Pina *et al*. (2014) proposed dissolution that is carrier controlled through their work with both completely and partially controlled amorphous dispersions [35]. It was observed that the type of polymer used had a significant effect on the dissolution compared to the morphology of the drug, partially crystalline formulations showed a higher rate of drug release in some cases compared to completely amorphous, therefore they proposed a controlled carrier mechanism. The drug release curves however in this study did not exhibit the spring and parachute effect, however they showed an increase in the drug concentration over 3 hours of dissolution. However it must be noted that a spring and parachute effect can still be seen as ASDs readily show a ‘’spring’’ and the parachute effect, may however be a slow parachute with supersaturation sustaining for many hours before precipitation starts to occur to define the parachute phase. It must be noted that all ASD formulations did not completely dissolve over the entire duration of the dissolution study. Therefore it is assumed that neither the polymer nor the drug completely dissolves over the 3 hours in pH buffer 1.2. Potter *et al*. (2015) prepared ASDs containing 10, 30 and 50% INM via supercritical fluid impregnation and hot melt extrusion and reported that polymer and INM did not completely dissolve even after 8 hours of dissolution [34].

The kinetic solubility of all ASD formulations increased compared to pure and amorphous INM (Figure 9). Amorphous and crystalline INM had a kinetic solubility of 2.4 µg/ml and 1.2 µg/ml as expected due to its conversion to the amorphous form. The increase in the kinetic solubility of INM was dependent upon both surfactant and polymeric carrier loading. The kinetic solubility of INM in this study increased by at least 10 times over 3 hours. Chokshi *et al*. (2008) prepared binary drug-polymer mixtures of PVP-VA64-INM using HME and achieved a maximum kinetic solubility of 10 µg/ml after 12 hours for all solid dispersions prepared using 70, 50 and 30% INM in pH buffer 1.2 [27].

It was also a significant improvement compared to the kinetic solubility of INM reported by Potter *et al*. (2015) [34] who prepared binary mixtures of INM and PVP via hot melt extrusion and supercritical fluid impregnation and achieved a maximum kinetic solubility of 8 µg/ml after 8 hours.

There was very little difference in terms of solubility between both the ternary ASD formulations and quaternary ASD formulations after 3 hours as shown in Figure 9. In this study PVP VA64 had the highest kinetic solubility with a value of 20.73 µg/ml (PVP VA64-SD4 (30% INM)) after 3 hours of dissolution. This was a similar result to the solubility from the previous study where the maximum solubility reported was 20 µg/ml with a 25% drug loading [30]. The ASDs with highest poloxamer loading had the highest solubility after 3 hours. This increase in solubility was related to the intermolecular interaction between drug and polymer and drug-polymer miscibility. The hydrophobic P407 propylene oxide core of the micelle which incorporated into the INM water-insoluble molecules also played a significant role in the increase in solubility of INM. P407 exists as a unimer self-assembled into micelles in solution [36]. This may have resulted in the increased kinetic solubility of INM molecules. P407 results in greater wetting and increases the surface that is available by reducing the interfacial tension between the dissolution medium and the poorly water- soluble drug. Reduced interfacial tension reduces the nucleation activation energy [37], therefore reducing recrystallization.

The AUC values of all ASD formulations was compared with pure and amorphous INM using a 1-way ANOVA and Tukey Kramer post hoc test (Figure 9). For both the quaternary, PL-S630 and PVP VA64 ternary ASD formulations with the exception of Quart SD2, Quart SD4, Quart SD7, Quart SD8, PVP VA64 SD2, PVP VA64 SD4, PL-S630 SD1, PL-S630 SD2 and PL-S630 SD4 there was no statistical difference between crystalline and amorphous INM. The overall effect of drug and % wt of poloxamer did have a significant effect on the solubility of INM and AUC in solution. After 3 hours, the ASD formulations did have a higher kinetic solubility compared to the pure and amorphous drug due to the conversion to the amorphous form (Figure 9). The samples that contained the highest drug loading recrystallized because of 1) the presence of crystalline INM, as it is higher to achieve the amorphous state using a high drug loading, 2) no inter-molecular interaction between drug and polymer and 3) drug-polymer immiscibility. For the quaternary mixtures only all ASDs with the highest % of poloxamer loading recrystallized with the exception of Quart SD4 and Quart SD8 as previously reported by Hurley *et al*. (2018) due to its gelling properties and its semi-crystalline nature of P407.

3.1.7 Accelerated stability studies

The 8 different combinations of ASD formulations were subjected to accelerated conditions of 40°C and 75% RH for 5 months, after which hyper DSC was performed to investigate the amorphous stability and to examine the crystalline content of each of the formulations as shown in Figure 10. Sinclair *et al*. (2011) reported the relative instability of all ASD formulations as a result of moisture uptake due to PVP which is very hygroscopic in nature [38]. It has been well documented in literature that water can act as a plasticizer and as a result lower the T_g of ASD formulations enhancing the molecular mobility of drugs and polymers.

Therefore prior to hyper DSC analysis all moisture was removed by drying the samples in a desiccator for 24 hours using phosphorus pentoxide as a desiccant.

The samples were dried as the moisture was coming off at the same temperature that the T_g occurred. After 5 months, all melt extrudates of the drug with PVP VA64, PL-S630 and P407 remained amorphous except for the 50% and 70% ASD formulations and showed no depression in T_g as a result of the moisture being removed compared to the initial T_g. This was also the case for Hurley *et al*. (2018) where ASDs were prepared with PVP VA64, P407 using INM as a model drug. All ASDs remained amorphous as a result of conversion from the crystalline to amorphous state as a result of the hydrogen bond interaction between drug and polymer, drug-polymer miscibility and due to the high molar attraction constant of INM. There was no depression in T_g after 5 months stability. This shows that all ASD formulations are miscible as predicted by the Hansen solubility parameters in Table 1. According to Couchman and Karasz, (1978) when drug and polymer are miscible the glass transition temperature of the extrudates will be between the glass transition temperatures of each of the pure components [39]. A single T_g was obtained for all formulations which is shown in Figure 10. It must be noted that a single T_g in ASD formulations may not be an indicator of a non-heterogeneous system. Qian *et al*. (2010) who reported may not always be a reliable indicator of homogeneity and optimal stability.

Qian *et al*. (2010) prepared two batches of ASDs using PVP VA64 and BMS-A as polymeric carriers and although two batches contained a distinctive single Tg, they exhibited crystallization and physical stability over time [40].

The higher drug load ASD formulations recrystallized as a result of the high drug loading as expected due to the following 1) the lack of inter-molecular interaction between drug and polymer at high drug loads, 2) the presence of INM in its crystalline form and 3) drug-polymer immiscibility. However as for the lower drug loads the drug remained amorphous which was similar to the data reported previously by Hurley *et al*. (2018) [30]. Hurley *et al*. (2018) prepared 5%, 10%, 15%, 20% and 25% INM ASD formulations and all ASD formulations remained amorphous and % P407 loading had no effect on the amorphous stability of INM [30].

4.1 Conclusion

The Hansen solubility parameters and drug-polymer interaction factor revealed the presence of intermolecular interactions between drug and polymer molecules. The findings from the XRPD studies showed that INM was molecularly dispersed and successfully incorporated within the hydrophilic PVP VA64 and PL-S630 matrix as a result of hot melt extrusion process and revealed the existence of possible

drug-polymer interactions. Except for the 50% and 70% ASD formulations which remained crystalline. ATR-FTIR and Raman studies confirmed the type and mechanism of interaction that occurred between amorphous INM and polymeric carriers. Hydrogen bonding between the C=O of the free carboxylic acid and amide carbonyl C=O of PVP VA64 and PL-S630.

Drug loading also had a significant effect with high drug loadings resulting in recrystallization of INM. It was observed that when Raman spectroscopy was performed, there was a shift in the vinyl acetate C=O carbonyl in all ASD formulations, however the quaternary ASD formulations had the greatest shift. This is very significant as it was reported by Yuan *et al*. (2015) that vinyl acetate C=O carbonyl is a weak hydrogen bond acceptor. Phase solubility studies of INM in aqueous solutions of PVP VA64, PL-S630 and P407 showed an increase in the kinetic solubility of INM compared to pure drug at 37°C in pH buffer 1.2 with a maximum K_a value of 0.12 µg/ml.

The ASD formulations showed a significantly higher dissolution rate compared to amorphous and pure INM in pH buffer 1.2 with a kinetic solubility of 24 µg/ml after 3 hours. After performing phase solubility studies for 24 hours on all ASD formulations, the maximum kinetic solubility reported was 73.60 µg/ml. This is very significant compared as the kinetic solubility of INM increased by at least 10 times over 3 hours compared to values reported in literature [27,34]. The kinetic solubility of the mixed PVP VA64 and PL-S630 systems was significantly higher than the ternary systems due to greater vinyl acetate hydrogen bonding interaction in the mixed copovidone blends.

The stability data showed that INM remained amorphous in solid solutions with PVP VA64 and PL-S630 except for the 50% and 70% INM ASD formulations, therefore % drug loading did have a significant effect on the amorphous stability of INM resulting in recrystallization for the higher drug loads. The samples with low drug loading remained amorphous as a result of the hydrogen bonding interaction between drug and polymer, drug-polymer miscibility as predicted by the Hansen solubility parameters, the melt temperatures used in the extrusion process, high molar attraction constant of INM and the surfactant properties of P407. This work illustrates the significance of utilizing quaternary and ternary drug-polymer intermolecular interactions by incorporating polymers with different crystallization inhibition mechanisms for to improve solid-state properties, dissolution properties and amorphous stability of BCS class II drugs such as INM. Also it also illustrates that 1) inter-molecular interactions and 2) mixed copovidone systems have a significant effect on the dissolution properties of INM. To improve the kinetic solubility of INM, formulation scientists have to carefully examine the role of inter-molecular interactions and the effect of solid-state properties and dissolution properties on the solubility of BCS class II drugs. In summary it's not just molecular interactions that improve the solubility of INM via the amorphous form, it is molecular

interactions in combination with correct preparation conditions/method, drug-polymer miscibility and nature of surfactants/polymeric carriers used that play a role in the successful formulation of amorphous solid dispersions.

Conflicts of Interest

The authors declare no competing financial interest.

Acknowledgments

This publication has emanated from research conducted with the financial support of the Synthesis and Solid State Pharmaceutical Centre, funded by Science Foundation Ireland under Grant 12/RC/2275 as well as support from University of Limerick (UL).

References

[1] N.J. Babu, A. Nangia, Solubility advantage of amorphous drugs and pharmaceutical cocrystals, Cryst. Growth Des. 11 (2011) 2662–2679. doi:10.1021/cg200492w.

[2] S.T. Buckley, K.J. Frank, G. Fricker, M. Brandl, Biopharmaceutical classification of poorly soluble drugs with respect to “enabling formulations,” Eur. J. Pharm. Sci. 50 (2013) 8–16. doi:10.1016/j.ejps.2013.04.002.

[3] D.H. Jornada, G.F. Dos Santos Fernandes, D.E. Chiba, T.R.F. De Melo, J.L. Dos Santos, M.C. Chung, The prodrug approach: A successful tool for improving drug solubility, Molecules. 21 (2016) 1–31. doi:10.3390/molecules21010042.

[4] M. Karashima, N. Sano, S. Yamamoto, Y. Arai, K. Yamamoto, N. Amano, Y. Ikeda, Enhanced pulmonary absorption of poorly soluble itraconazole by micronized cocrystal dry powder formulations., Eur. J. Pharm. Biopharm. 115 (2017) 65–72.

[5] D.D. Sun, P.I. Lee, Probing the mechanisms of drug release from amorphous solid dispersions in medium-soluble and medium-insoluble carriers, J. Control. Release. 211 (2015) 85–93. doi:10.1016/j.jconrel.2015.06.004.

[6] T. Shah, T. Laaksonen, T. Rades, J. Aaltonen, L. Peltonen, C. Strachan, Unravelling the Relationship between Degree of Disorder and the Dissolution Behavior of Milled Glibenclamide, Mol. Pharm. 11 (2013) 234–242.

[7] S. Baghel, H. Cathcart, N.J. O’Reilly, Polymeric Amorphous Solid Dispersions: A Review of

Amorphization, Crystallization, Stabilization, Solid-State Characterization, and Aqueous Solubilization of Biopharmaceutical Classification System Class II Drugs, J. Pharm. Sci. 105 (2016) 2527–2544. doi:10.1016/j.xphs.2015.10.00810.1021/mp500644h.

[8] S. Baghel, H. Cathcart, W. Redington, N. O'Reilly, An investigation into the crystallization tendency/kinetics of amorphous active pharmaceutical ingredients: A case study with dipyridamole and cinnarizine., Eur. J. Pharm. Biopharm. 104 (2016) 59–71.

[9] E. Amstad, F. Spaepen, D. Weitz, Stabilization of the Amorphous Structure of Spray-Dried Drug Nanoparticles, J. Phys. Chem. B. 120 (2016) 9161–9165.

[10] T. Xie, L. Taylor, Dissolution Performance of High Drug Loading Celecoxib Amorphous Solid Dispersions Formulated with Polymer Combinations., Pharm. Res. 33 (2016) 739–750.

[11] M.A. Altamimi, S.H. Neau, Use of the Flory-Huggins theory to predict the solubility of nifedipine and sulfamethoxazole in the triblock, graft copolymer Soluplus, Drug Dev. Ind. Pharm. 42 (2016) 446–455. doi:10.3109/03639045.2015.1075033.

[12] M. Maniruzzaman, M.J. Snowden, M.S. Bradely, D. Douroumis, Studies of intermolecular interactions in solid dispersions using advanced surface chemical analysis, RSC Adv. 5 (2015) 74212–74219. doi:10.1039/C5RA13176F.

[13] L.S. Taylor, G. Zografi, Spectroscopic characterization of interactions between PVP and indomethacin in amorphous molecular dispersions, Pharm. Res. 14 (1997) 1691–1698. doi:10.1023/A:1012167410376.

[14] T. Matsumoto, G. Zografi, Physical Properties of Solid Molecular Dispersions of Indomethacin with Poly(vinylpyrrolidone) and Poly(vinylpyrrolidone-co-vinyl-acetate) in Relation to Indomethacin Crystallization, Pharm. Res. 16 (1999) 1722–1728.

[15] P.J. Marsac, H. Konno, L.S. Taylor, A comparison of the physical stability of amorphous felodipine and nifedipine systems, Pharm. Res. 23 (2006) 2306–2316. doi:10.1007/s11095-006-9047-9.

[16] T. Miyoshi, K. Takegoshi, K. Hikichi, High-resolution solid state 13C n.m.r. study of the interpolymer interaction, morphology and chain dynamics of the poly(acrylic acid)/ poly(ethylene oxide) complex, Polymer (Guildf). 38 (1997) 2315–2320. doi:10.1016/S0032-3861(96)00799-9.

[17] X. Yuan, T.-X. Xiang, B.D. Anderson, E.J. Munson, Hydrogen Bonding Interactions in Amorphous Indomethacin and Its Amorphous Solid Dispersions with Poly(vinylpyrrolidone) and Poly(vinylpyrrolidone-co-vinyl acetate) Studied Using 13 C Solid-State NMR, Mol. Pharm. 12 (2015) 4518–4528. doi:10.1021/acs.molpharmaceut.5b00705.

[18] S. Baghel, H. Cathcart, N.J. O'Reilly, Investigation into the Solid-State Properties and Dissolution Profile of Spray-Dried Ternary Amorphous Solid Dispersions: A Rational Step toward the Design and Development of a Multicomponent Amorphous System, Mol. Pharm. 15 (2018) 3796–3812. doi:10.1021/acs.molpharmaceut.8b00306.

[19] X. Wang, A. Michoel, G. Van Den Mooter, Solid state characteristics of ternary solid dispersions composed of PVP VA64, Myrj 52 and itraconazole, Int. J. Pharm. 303 (2005) 54–61. doi:10.1016/j.ijpharm.2005.07.002.

[20] F. Damian, N. Blaton, R. Kinget, M. Van de Mooter, Physical stability of solid dispersions of the antiviral agent UC-781 with PEG 6000, Gelucire 44/14 and PVP K30., Int. J. Pharm. 244 (2002) 87–89.

[21] F. Tres, K. Treacher, J. Booth, L.P. Hughes, S.A.C. Wren, J.W. Aylott, J.C. Burley, Indomethacin-Kollidon VA64 Extrudates: A Mechanistic Study of pH-Dependent Controlled Release, Mol. Pharm. (2016). doi:10.1021/acs.molpharmaceut.5b00979.

[22] M. Maniruzzaman, M.M. Rana, J.S. Boateng, J.C. Mitchell, D. Douroumis, Dissolution enhancement of poorly water-soluble APIs processed by hot-melt extrusion using hydrophilic polymers, Drug Dev. Ind. Pharm. 39 (2012) 218–227. doi:10.3109/03639045.2012.670642.

[23] H. Hildebrand, S. Scott, The Solubility of Nonelectrolytes, Reinhold Publishing Coporation, New York, USA, 1950.

[24] T. Higuchi, K. Connors, Phase-solubility techniques, Adv. Anal. Chem. Instrum. 4 (1965) 117–212.

[25] T. Hansen, P. Holm, K. Schultz, Process characteristics and compaction of spray-dried emulsions containing a drug dissolved in lipid, Int. J. Pharm. 287 (2004) 55–66. doi:10.1016/j.ijpharm.2004.08.014.

[26] E.R. Gaikwad, S.S. Khabade, T.B. Sutar, M.R. Bhat, S. Ambadas Payghan, Three-dimensional

626 Hansen Solubility Parameters as Predictors of Miscibility in Cocrystal Formation, Asian J. Pharm.
627 @BULLET. 11 (2017) 302–318. doi:10.22377/AJP.V11I04.1627.

628 [27] R.J. Chokshi, N.H. Shah, H.K. Sandhu, A.W. Malick, H. Zia, Stabilization of low glass transition
629 temperature indomethacin formulations: Impact of polymer-type and its concentration, J. Pharm.
630 Sci. 97 (2008) 2286–2298. doi:10.1002/jps.21174.

631 [28] S.G. Gumaste, S.S. Gupta, A.T.M. Serajuddin, Investigation of Polymer-Surfactant and Polymer-
632 Drug-Surfactant Miscibility for Solid Dispersion., AAPS J. 18 (2016). doi:10.1208/s12248-016-
633 9939-5.

634 [29] S.Y. Chan, Y.Y. Chung, X.Z. Cheah, E.Y.L. Tan, J. Quah, The characterization and dissolution
635 performances of spray dried solid dispersion of ketoprofen in hydrophilic carriers, Asian J. Pharm.
636 Sci. 10 (2015) 372–385. doi:10.1016/j.ajps.2015.04.003.

637 [30] D. Hurley, C.B. Potter, G.M. Walker, C.L. Higginbotham, Investigation of Ethylene Oxide-co-
638 propylene Oxide for Dissolution Enhancement of Hot-Melt Extruded Solid Dispersions, J. Pharm.
639 Sci. 107 (2018) 1372–1382. doi:10.1016/j.xphs.2018.01.016.

640 [31] M. Newa, K.H. Bhandari, D.H. Oh, Y.R. Kim, J.H. Sung, J.O. Kim, J.S. Woo, H.G. Choi, C.S.
641 Yong, Enhanced dissolution of ibuprofen using solid dispersion with poloxamer 407, Arch.
642 Pharm. Res. 31 (2008) 1497–1507. doi:10.1007/s12272-001-2136-8.

643 [32] H. Shekhar, V. Kant, Thermodynamic investigation on solid dispersions of nicotinamide –
644 sulphamerazine drug system, Sci. World. 11 (2013) 52–57. doi:10.1080/15421406.2013.782207.

645 [33] S.S. Jambhekar, P. Breen, Cyclodextrins in pharmaceutical formulations I: Structure and
646 physicochemical properties, formation of complexes, and types of complex, Drug Discov. Today.
647 21 (2016) 356–362. doi:10.1016/j.drudis.2015.11.017.

648 [34] C. Potter, Y. Tian, G. Walker, C. McCoy, P. Hornsby, C. Donnelly, D.S. Jones, G.P. Andrews,
649 Novel supercritical carbon dioxide impregnation technique for the production of amorphous solid
650 drug dispersions: A comparison to hot melt extrusion, Mol. Pharm. 12 (2015) 1377–1390.
651 doi:10.1021/mp500644h.

652 [35] M.F. Pina, M. Zhao, J.F. Pinto, J.J. Sousa, D.Q.M. Craig, The influence of drug physical state on
653 the dissolution enhancement of solid dispersions prepared via hot-melt extrusion: A case study
654 using olanzapine, J. Pharm. Sci. 103 (2014) 1214–1223. doi:10.1002/jps.23894.

[36] V. Vyas, P. Sancheti, P. Karekar, M. Shah, Y. Pore, Physicochemical characterization of solid dispersion systems of tadalafil with poloxamer 407, Acta Pharm. 4 (2009) 453–461. doi:10.2478/v10007-009-0037-4.

[37] G.A. Ilevbare, H. Liu, K.J. Edgar, L.S. Taylor, Effect of binary additive combinations on solution crystal growth of the poorly water-soluble drug, ritonavir, Cryst. Growth Des. 12 (2012) 6050–6060. doi:10.1021/cg301169t.

[38] W. Sinclair, M. Leane, G. Clarke, A. Dennis, M. Tobyn, P. Timmins, Physical Stability and Recrystallization Kinetics of Amorphous Ibipinabant Drug Product by Fourier Transform Raman Spectroscopy, J. Pharm. Sci. 100 (2011) 4687–4699. doi:10.1002/jps.22658.

[39] P.R. Couchman, F.E. Karasz, A Classical Thermodynamic Discussion of the Effect of Composition on Glass-Transition Temperatures, Macromolecules. 11 (1978) 117–119. doi:10.1021/ma60061a021.

[40] F. Qian, J. Huang, Q. Zhu, R. Haddadin, J. Gawel, R. Garmise, M. Hussain, Is a distinctive single Tg a reliable indicator for the homogeneity of amorphous solid dispersion?, Int. J. Pharm. 395 (2010) 232–235. doi:10.1016/j.ijpharm.2010.05.033.

List of tables

Table 3. Calculated Hansen solubility and F-H interaction parameters for INM and each polymer.

Table 4. Gibbs free energy Values and Apparent stability constants (K_a) of ternary and quaternary drug-polymer-surfactant interactions.

Table 5. Comparison of the solubility of INM from various quaternary and ternary ASD formulations and corresponding physical mixtures in pH buffer 1.2 after 3 and 24 hours respectively.

Table 1

Batch No	**Composition (% w/w)**			
	PL-S630 (%w/w)	**PVP VA64 (% w/w)**	**P407 (% w/w)**	**INM (% w/w)**
Quart SD1	42.5	42.5	5	10
Quart SD2	37.5	37.5	15	10

Quart SD3	32.5	32.5	5	30
Quart SD4	27.5	27.5	15	30
Quart SD5	22.5	22.5	5	50
Quart SD6	17.5	17.5	15	50
Quart SD7	12.5	12.5	5	70
Quart SD8	7.5	7.5	15	70

Table 2

Identifier	**Composition (% w/w)**		
	PL-S630/PVP VA64	**P407 (% w/w)**	**INM (% w/w)**

	(%w/w)		
PL-S630/PVP VA64 SD1	85	5	10
PL-S630/PVP VA64 SD2	75	15	10
PL-S630/PVP VA64 SD3	65	5	30
PL-S630/PVP VA64 SD4	55	15	30
PL-S630/PVP VA64 SD5	45	5	50
PL-S630/PVP VA64 SD6	35	15	50
PL-S630/PVP VA64 SD7	25	5	70
PL-S630/PVP VA64 SD8	15	15	70

Table 3

Compound	δ_t (MPa$^{1/2}$)	$\Delta\delta$ (MPa$^{1/2}$)	χ
INM	23.00	-	-
PVP VA64	26.40	3.40	0.46
PL-S630	26.40	3.40	0.46
P407	25.50	2.50	0.36

Table 4

758

Concentration of P407 (%wt/vol)	Concentration of PL-S630 (%wt/vol)	Concentration of PVP VA64 (%wt/vol)	Quantity of INM added (mg)	Combined Concentration of Polymer (% wt/vol)	ΔG^{0}_{tr} (kJ/mol)		
					PL-S630+P407	PVP VA64+P407	Quaternary
5	5	5	50	5	1.56	0.58	0.23
7.5	25	25	50	25	-1.37	-1.07	-0.94
10	45	45	50	45	-2.27	-1.87	-1.63
12.5	65	65	50	65	-2.64	-2.57	-2.35
15	85	85	50	85	-3.78	-2.72	-2.56
		Intercept			1.90×10^{0}	5.42×10^{0}	5.96×10^{0}
		Slope			0.30×10^{0}	0.19×10^{0}	0.16×10^{0}
		K_a (µg/ml)			0.12	0.04	0.03

759

760

761

762

763

764

765

766

767

768

769

770

771

772

773 **Table 5**

Formulation	Solubility of INM (µg/ml) after 3 hrs.	Solubility of INM (µg/ml) after 24 hrs.	
	ASD	Physical Mixture	ASD
PVP VA64 SD1	4.43	4.57	11.20
PVP VA64 SD2	7.90	21.23	5.67
PVP VA64 SD3	7.80	21.93	4.00
PVP VA64 SD4	20.73	26.50	2.13
PVP VA64 SD5	6.86	29.17	1.50
PVP VA64 SD6	9.20	19.77	4.17
PVP VA64 SD7	1.33	18.83	0.93
PVP VA64 SD8	6.47	16.23	6.73
PL-S630 SD1	13.83	4.40	14.00
PL-S630 SD2	14.03	14.80	14.00
PL-S630 SD3	8.40	7.77	6.43
PL-S630 SD4	10.60	11.57	10.60
PL-S630 SD5	0.50	7.63	4.37
PL-S630 SD6	3.37	6.70	8.07
PL-S630 SD7	2.03	7.27	6.90
PL-S630 SD8	2.83	7.13	4.50
Quart SD1	6.40	53.87	73.60
Quart SD2	12.67	45.63	31.23
Quart SD3	5.50	26.13	23.47
Quart SD4	8.03	24.30	34.17
Quart SD5	4.30	29.00	16.77
Quart SD6	4.87	22.57	14.13
Quart SD7	9.43	20.23	16.53
Quart SD8	9.53	18.50	21.17

List of figures

Figure 10. Hyper DSC traces of ASD formulations after 5 months stability study under accelerated aging conditions of 40°C and 75% RH. The heating rate used was 100°C/min. The area of interest of the γ-INM melting endotherm is marked by solid lines. **T_g is indicated by a tick.**

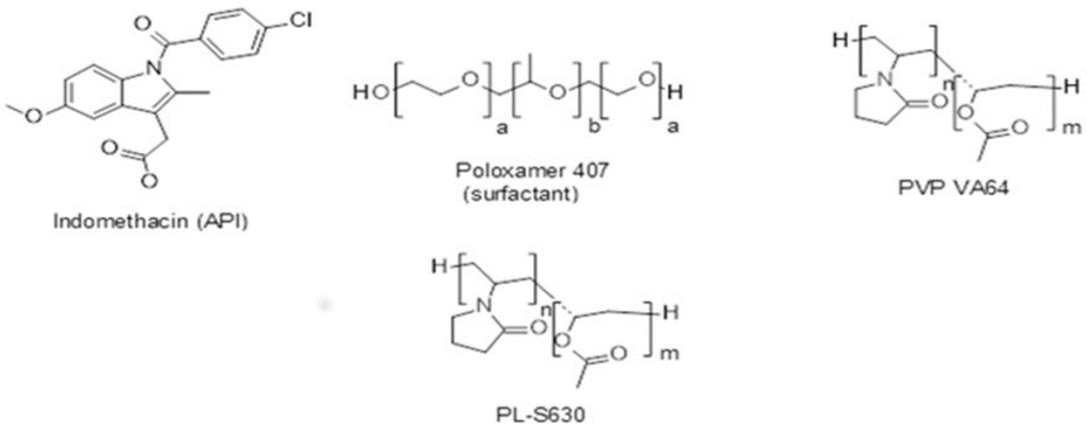
Indomethacin (API)
Poloxamer 407
(surfactant)
PVP VA64
PL-S630

Figure 1

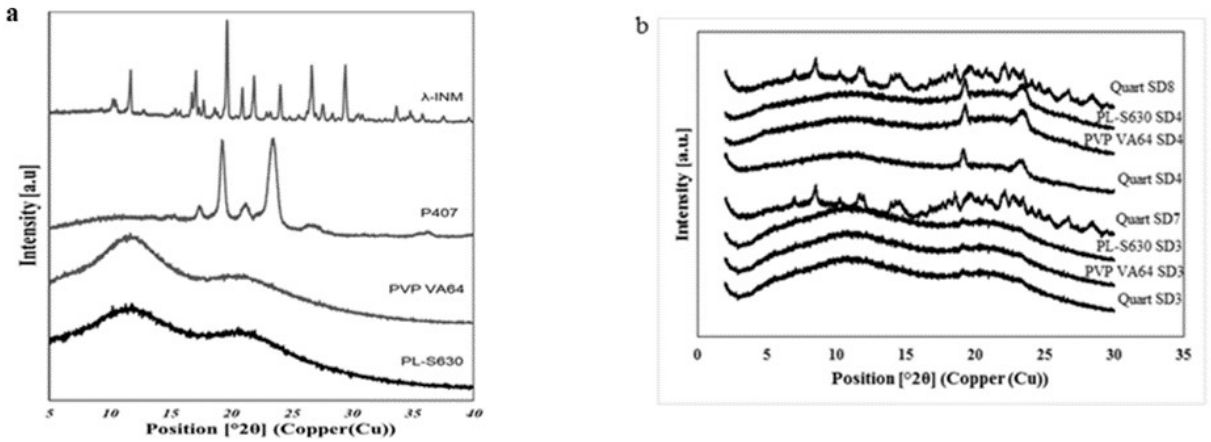
a
λ-INM
P407
PVP VA64
PL-S630
Intensity [a.u]
5 10 15 20 25 30 35 40
Position [°2θ] (Copper(Cu))
b
Quart SD8
PL-S630 SD4
PVP VA64 SD4
Quart SD4
Quart SD7
PL-S630 SD3
PVP VA64 SD3
Quart SD3
Intensity [a.u.]
0 5 10 15 20 25 30 35
Position [°2θ] (Copper (Cu))

Figure 2.

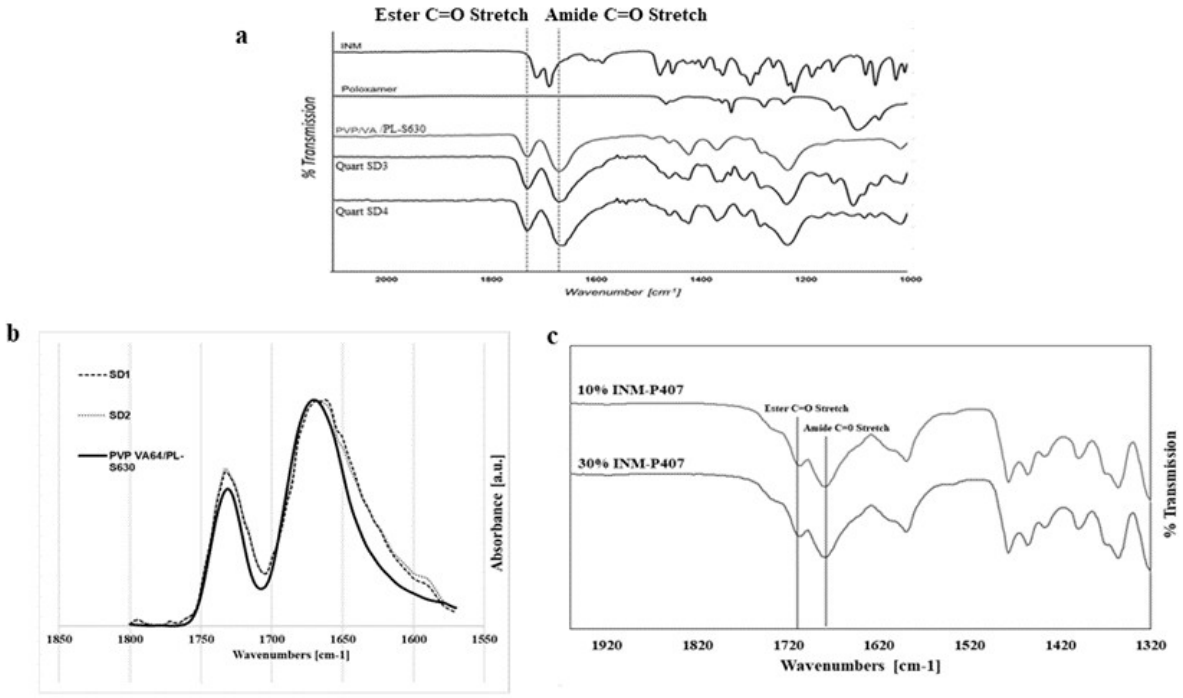
a
Ester C=O Stretch
Amide C=O Stretch
INM
Poloxamer
PVP/VA /PL-S630
Quart SD3
Quart SD4
% Transmission
2000
1800
1600
1400
1200
1000
Wavenumber [cm⁻¹]
b
SD1
SD2
PVP VA64/PL-S630
Absorbance [a.u.]
1850
1800
1750
1700
1650
1600
1550
Wavenumbers [cm-1]
c
10% INM-P407
30% INM-P407
Ester C=O Stretch
Amide C=O Stretch
% Transmission
1920
1820
1720
1620
1520
1420
1320
Wavenumbers [cm-1]

Figure 3.

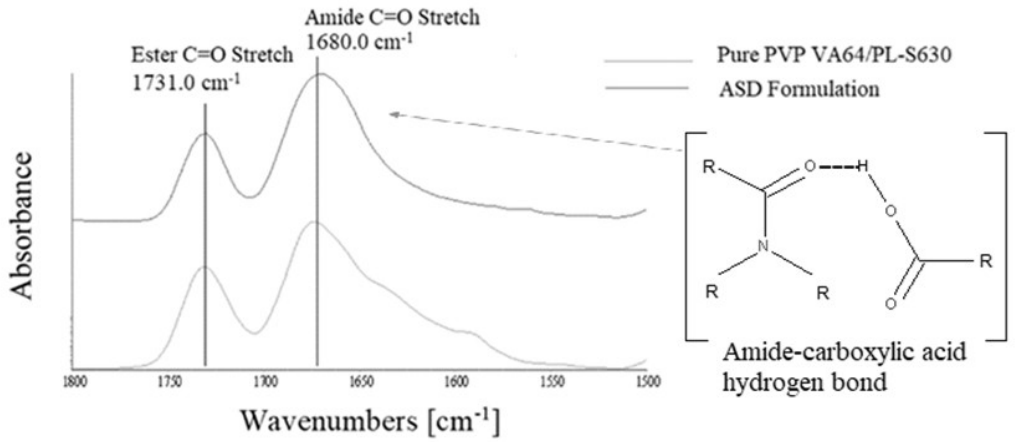
Amide C=O Stretch
1680.0 cm-1
Ester C=O Stretch
1731.0 cm-1
Pure PVP VA64/PL-S630
ASD Formulation
Absorbance
1800
1750
1700
1650
1600
1550
1500
Wavenumbers [cm-1]
R
O
H
N
R
R
O
O
R
Amide-carboxylic acid
hydrogen bond

Figure 4.

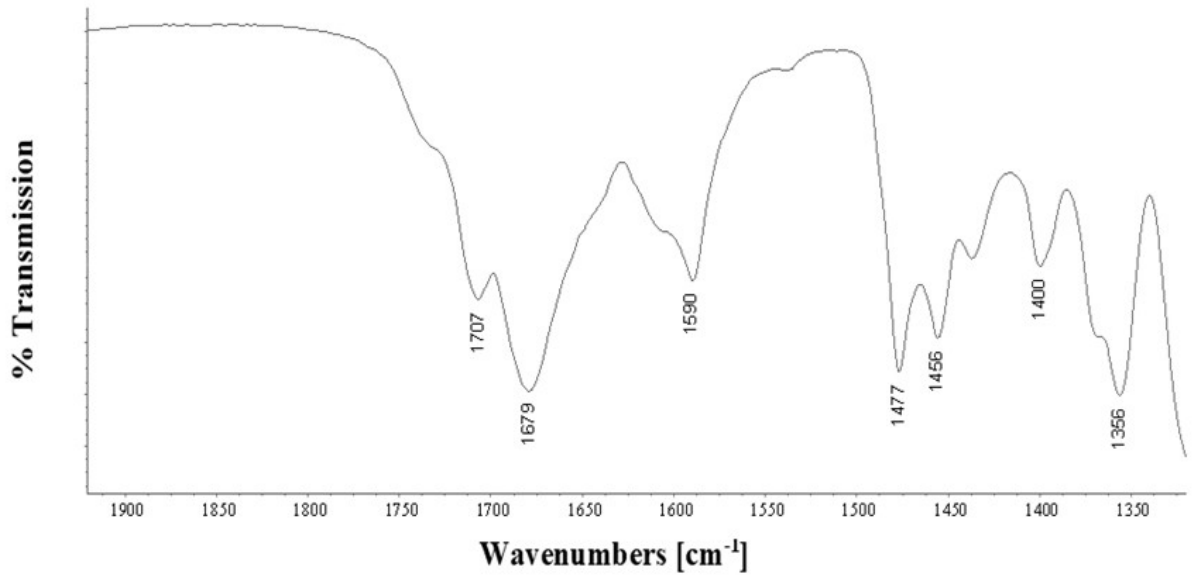
% Transmission
1707
1679
1590
1477
1456
1400
1356
1900
1850
1800
1750
1700
1650
1600
1550
1500
1450
1400
1350
Wavenumbers [cm-1]

Figure 5.

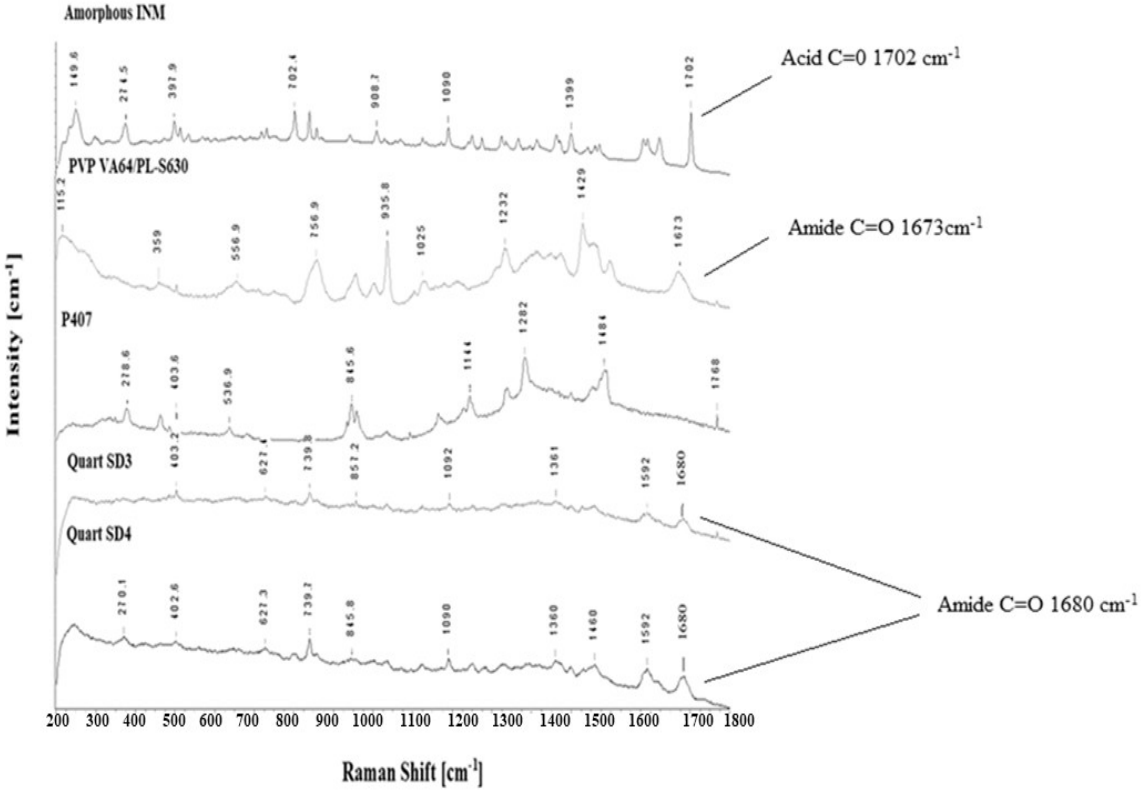
Amorphous INM
PVP VA64/PL-S630
P407
Quart SD3
Quart SD4
Acid C=0 1702 cm-1
Amide C=O 1673cm-1
Amide C=O 1680 cm-1
Intensity [cm-1]
Raman Shift [cm-1]
200 300 400 500 600 700 800 900 1000 1100 1200 1300 1400 1500 1600 1700 1800

Figure 6.

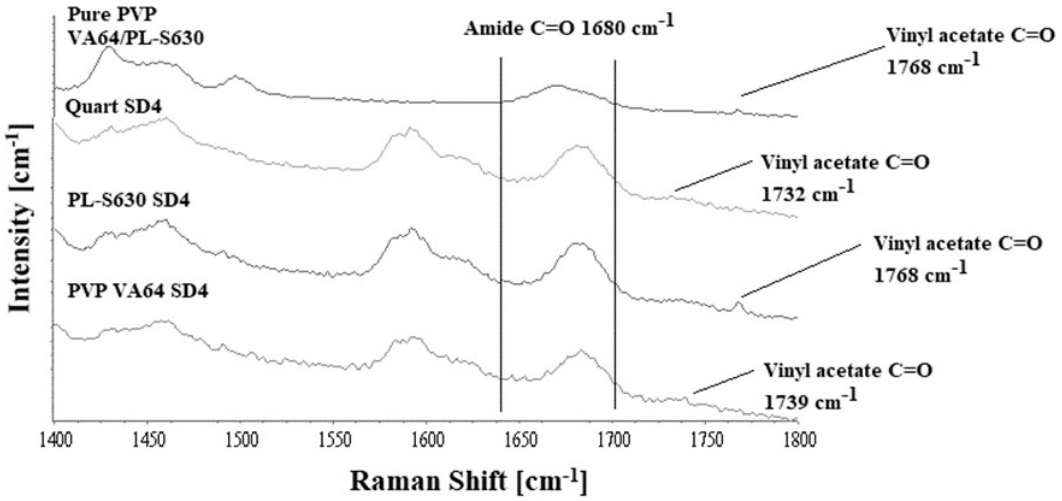
Pure PVP
VA64/PL-S630
Amide C=O 1680 cm-1
Vinyl acetate C=O
1768 cm-1
Quart SD4
Vinyl acetate C=O
1732 cm-1
PL-S630 SD4
Vinyl acetate C=O
1768 cm-1
PVP VA64 SD4
Vinyl acetate C=O
1739 cm-1
Intensity [cm-1]
1400
1450
1500
1550
1600
1650
1700
1750
1800
Raman Shift [cm-1]

Figure 7.

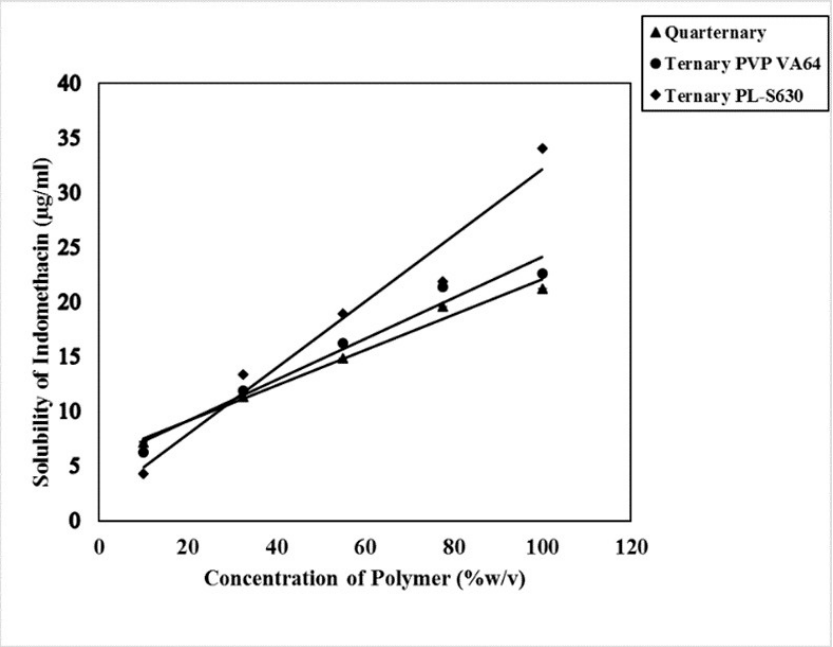

952

953 **Figure 8.**

954

955

956

957

958

959

960

961

962

963

964

965

966

967

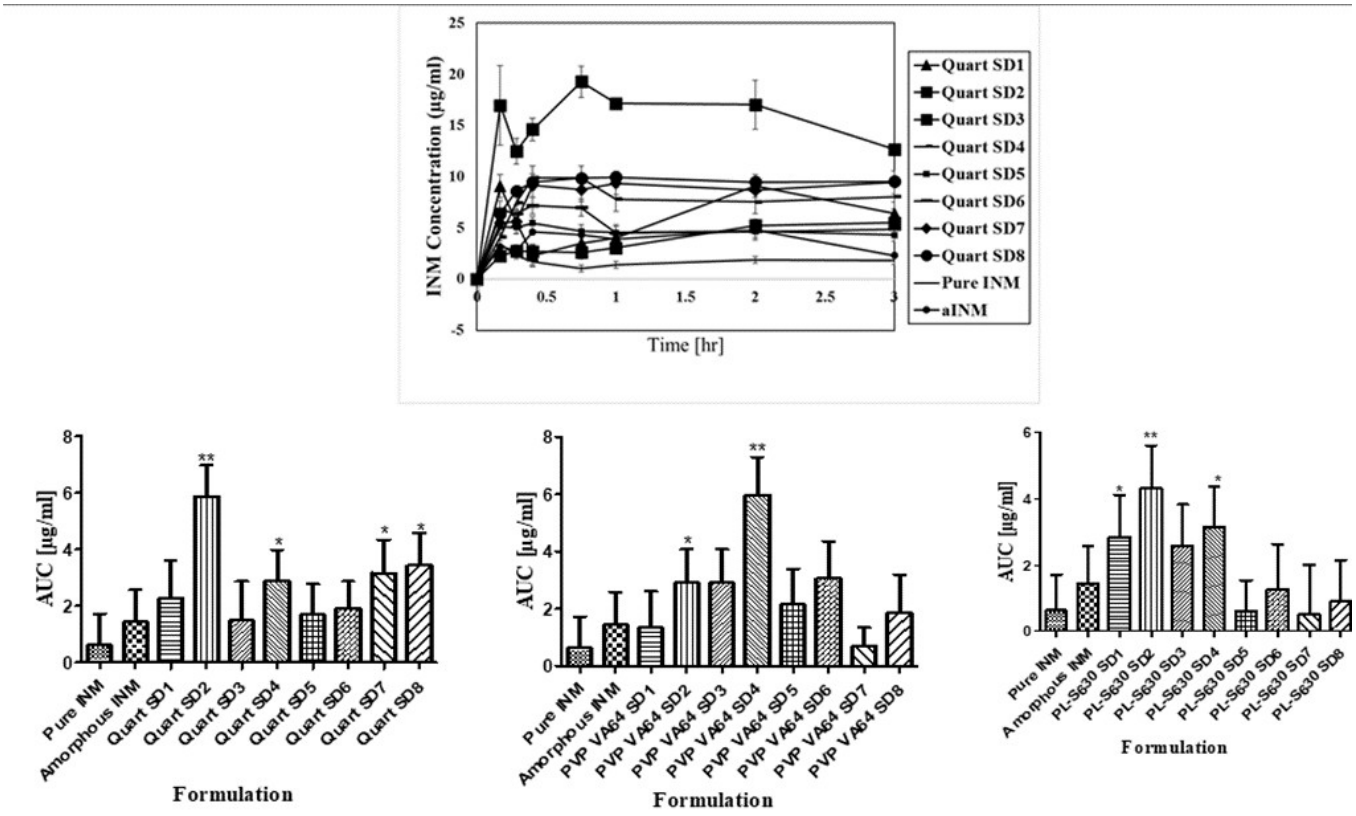
INM Concentration (µg/ml)
Time [hr]
Quart SD1
Quart SD2
Quart SD3
Quart SD4
Quart SD5
Quart SD6
Quart SD7
Quart SD8
Pure INM
aINM
AUC [µg/ml]
Formulation
Pure INM
Amorphous INM
Quart SD1
Quart SD2
Quart SD3
Quart SD4
Quart SD5
Quart SD6
Quart SD7
Quart SD8
PVP VA64 SD1
PVP VA64 SD2
PVP VA64 SD3
PVP VA64 SD4
PVP VA64 SD5
PVP VA64 SD6
PVP VA64 SD7
PVP VA64 SD8
PL-S630 SD1
PL-S630 SD2
PL-S630 SD3
PL-S630 SD4
PL-S630 SD5
PL-S630 SD6
PL-S630 SD7
PL-S630 SD8

Figure 9.

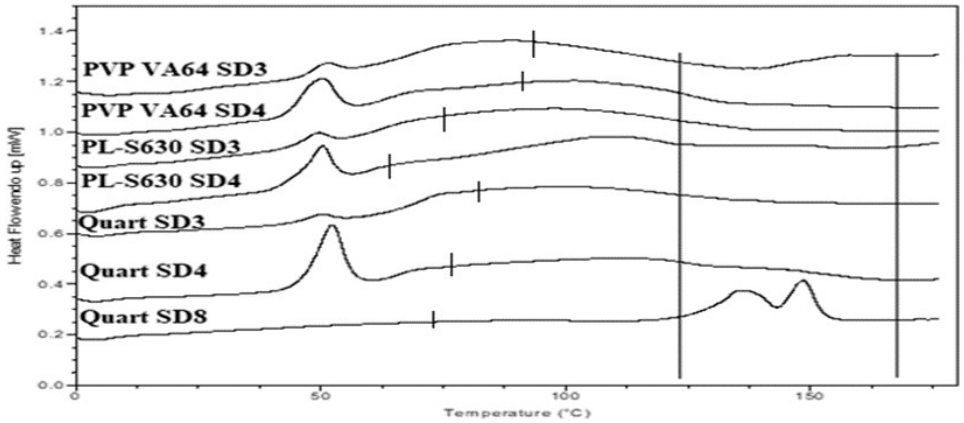
PVP VA64 SD3
PVP VA64 SD4
PL-S630 SD3
PL-S630 SD4
Quart SD3
Quart SD4
Quart SD8
Heat Flowendo up [mW]
Temperature (°C)
0.0
0.2
0.4
0.6
0.8
1.0
1.2
1.4
0
50
100
150

Figure 10.

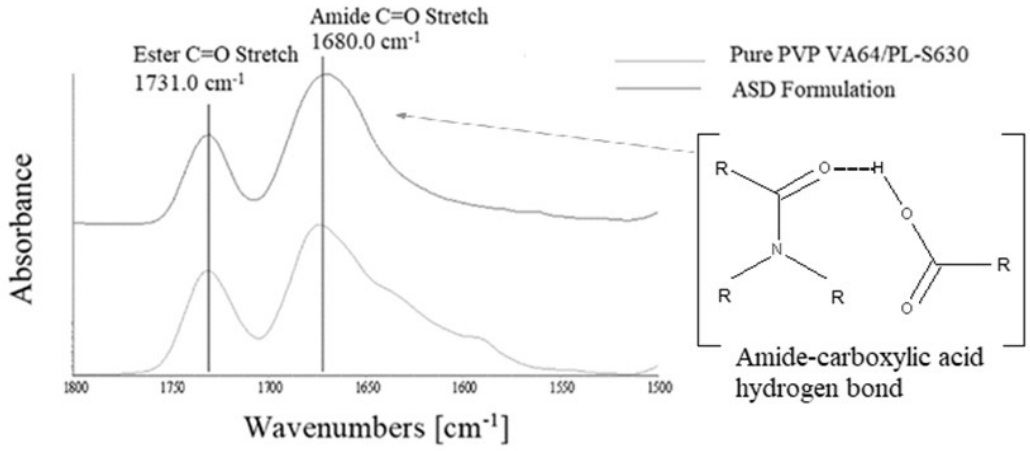

999

1000 **Graphical Abstract**

1001

1002

1003

1004

1005

1006

1007

1008

1009

1010

1011

1012

1013

1014

1015

1016

Supporting Information

An investigation of the intermolecular interaction, solid-state properties and dissolution properties of mixed copovidone hot-melt extruded solid dispersions

Dean Hurley[1, 2], David Carter[1], Lawrence Yee Foong Ng[1], Mark Davis[2], Gavin M. Walker[2], John G. Lyons[1], Clement L. Higginbotham[1, 2*]

[1]Materials Research Institute, Athlone Institute of Technology, Athlone, Ireland

[2]Synthesis and Solid State Pharmaceutical Centre (SSPC), Bernal Institute, University of Limerick, Limerick, Ireland.

List of Tables

Table 6. Interpretation of ATR-FTIR Spectrum of indomethacin

Bond Vibration	Frequency (cm^{-1})
C-Cl Stretch	751.01
-COOH out of plane Stretch	924.22
C-O Stretch	1222.22
O-CH_3 Stretch	1453.61
Aromatic C=C Stretch	1588.10
C=O Stretch (Two bands)	1689.62, 1712.67
Aromatic C-H Stretch, -COOH (superimposed)	2927.60

Table 7. Interpretation of ATR-FTIR Spectrum of PVP VA64/PL-S630.

Bond Vibration	Frequency (cm^{-1})
C-O Stretch (Two bands)	1019.22, 1234.09
Ester C=O Stretch	1730.88
Amide C=O Stretch	1672.00
C-N Stretch of amine	1369.30
Alkyl C-H Stretch	3100.00
C-H bending	1422.92

Table 8. Interpretation of ATR-FTIR Spectrum of Poloxamer 407.

Bond Vibration	Frequency (cm^{-1})
Aliphatic C-H Stretch (Two bands)	2978.76, 2883.93
In plane O-H bend	1342.20
C-O Stretch	1099.59

Table 9. Interpretation of ATR-FTIR Spectrum of ASD formulations.

Bond Vibration	Frequency (cm^{-1})
C-O Stretch (Two bands)	1019.22, 1234.09
Ester C=O Stretch	1730.88
Amide C=O Stretch	1680.00
C-N Stretch of amine	1369.30
Alkyl C-H Stretch	3100.00
C-H bending	1422.92

Table 10. Interpretation of Raman Spectrum of indomethacin

Bond Vibration	Frequency (cm^{-1})
***v*C-Cl Stretch**	702.40
δCH_3	1399.00
***v*(C-O-C) asym**	1090.00
***v*(C-O-C)**	906.30
Amide *v*C=O Stretch	1680.00
Acid *v*C=O	1702.00

Table 11. Interpretation of Raman Spectrum of PVP VA64/PL-S630

Bond Vibration	Frequency (cm^{-1})
***v*(C-O-C)**	935.6
***v*(C-O-C) asym**	1026.00
***v*(CC), aliphatic chain vibrations**	1232.00
δCH_3 asym	1420.00
δCH_2	1423.00
Amide *v*C=O Stretch	1673.00
Vinyl acetate *v*C=O	1768.00

Table 12. Interpretation of Raman Spectrum of Poloxamer 407

Bond Vibration	Frequency (cm^{-1})
***v*(C-O-C)**	845.6
***v*(C-O-C) asym**	1145.00
***v*(CC), aliphatic chain vibrations**	1202.00
δCH_3 asym	1484.00
δCH_2	1482.00

Table 13. Interpretation of Raman Spectrum of a selected ASD formulations (Quart SD4).

Bond Vibration	Frequency (cm^{-1})
***v*(C-O-C)**	845.80
***v*(C-O-C) asym**	1092.00
δCH_3 asym	1460.00
δCH_2	1458.00
***v*C-N Stretch**	1592.00
Amide *v*C=O Stretch	1680.00
Vinyl acetate *v*C=O	1732.00